Evolution of density fluctuations to lamellar crystals in linear polyethylene

Yvonne A. Akpalu and Eric J. Amis

Citation: The Journal of Chemical Physics **111**, 8686 (1999); doi: 10.1063/1.480208
View online: http://dx.doi.org/10.1063/1.480208
View Table of Contents: http://scitation.aip.org/content/aip/journal/jcp/111/18?ver=pdfcov
Published by the AIP Publishing

Evolution of density fluctuations to lamellar crystals in linear polyethylene

Yvonne A. Akpalu and Eric J. Amis[a)]
Polymers Division, National Institute of Standards and Technology, Gaithersburg, Maryland 20899

(Received 16 March 1999; accepted 9 August 1999)

Structure formation during the isothermal crystallization of a linear polyethylene ($M_w = 32\,100$ g/mol, $M_w/M_n = 1.1$) has been monitored by simultaneous real time small-angle x-ray scattering (SAXS) and wide angle x-ray scattering (WAXS) with synchrotron radiation. Changes in the crystalline and amorphous scattering in WAXS occur simultaneously with the changes observed in the SAXS intensity profile, suggesting that the resulting scattering is a consequence of forming crystals. At the early stage of crystal growth, the SAXS intensity at $q < 0.02\,\text{Å}^{-1}$ increases while that at higher wave vectors remains constant. Meanwhile, the apparent crystallinity from WAXS increases to about 10% before two peaks in the SAXS intensity profile can be resolved. As lamellar stacks develop, the period corresponding to the first SAXS peak, L_1, decreases initially. After reaching a minimum, L_1 further increases with crystallization time. On the other hand, the period corresponding to the second SAXS peak increases with crystallization time. At late times, the rate of increase is very slow. Changes in the crystallinity obtained from WAXS and the total scattering power from SAXS were evaluated and compared with a model for the crystallizing system which accounts for changes in the fraction of lamellar aggregates. The relative importance of two secondary crystallization processes, namely the formation of new lamellar stacks and increase in the crystallinity within lamellae, were evaluated during and after primary crystallization. © *1999 American Institute of Physics.* [S0021-9606(99)51441-4]

I. INTRODUCTION

Crystalline polymers show ordering at different size scales, namely, the arrangement of molecules in the unit cell, lamellar crystals and the aggregation of these lamellae into superstructures such as spherulites and axialites.[1,2] In the classical picture of polymer crystallization,[3] nucleation occurs when the polymer solution or melt is supercooled. The process is initiated by large-amplitude, local fluctuations of an order parameter such as density. The result is the appearance of small nuclei of the stable crystalline phase and only those that are larger than a critical size grow. There is an induction time τ_c, associated with the time to form the critical crystal nuclei from the amorphous state. The primary lamellar habit is formed as a result of the anisotropic growth of nuclei. For the nucleation and growth mechanism, Bragg peaks in the wide-angle x-ray scattering (WAXS), corresponding to isolated crystals, will evolve first. As lamellar stacks are developed, scattering maxima in the small-angle x-ray scattering (SAXS) will appear.

Time-resolved x-ray scattering studies on polyethylene,[4–7] show that the crystallization of polyethylene from the melt state can be described by two stages: (1) Primary crystallization with the growth of superstructures, and (2) secondary crystallization during which the degree of crystallinity within the morphological units increases. Although a distinction between primary and secondary crystallization can be made, usually the two processes cannot be delineated. However, by comparing the time evolution of the degree of crystallinity obtained from WAXS and the total scattering power obtained from SAXS it may be possible to identify and separate the crystallization mechanisms in the samples under study.

On the other hand, a mechanism different from nucleation and growth has been proposed during the crystallization of poly(ethylene teraphlate) (PET),[8–10] poly(ether ketone ketone) (PEEK)[11] and isotatic polypropylene (*i*)-PP.[12] For PET and PEEK, structural changes in these samples were monitored while the samples were annealed above the glass transition temperature, T_g, from a melt-quenched glass. These experiments show the development of a SAXS peak, due to electron density fluctuations, prior to the presence of crystals identified by WAXS. Initially, the SAXS peak intensity grows exponentially with time while the corresponding wave vector remains constant. This scattering behavior is consistent with the Cahn–Hilliard[13] theory for early stage spinodal decomposition. During the late stage of the induction period the scattering behavior of PET is consistent with predictions of the Furukawa scaling theory for the late stages of spinodal decomposition. Further domain growth is arrested when Bragg peaks emerge in the WAXS profile. The characteristic size of the ordered domains formed before crystals can be identified by WAXS is usually larger than the lamellar thickness after crystallization is complete. Recently Olmsted and co-workers[14] have proposed a theory based on the coupling of density and chain conformation to describe these observations. They proposed that this coupling induces a liquid–liquid binodal within the equilibrium liquid–crystalline solid coexistence curve and if a polymer melt is quenched below the spinodal, it will phase separate into two co-existing liquids which differ in their distribution of conformations. The characteristic length scale associated with

a)Electronic mail: eric.amis@nist.gov

the developing spinodal texture gives rise to a SAXS peak and the growth of this peak is arrested once Bragg peaks appear in the WAXS intensity profile.

For rigid rod polymers such as PET and PEEK, earlier calculations[15–17] indicate that orientational ordering in the polymer melt can occur when the stiffness of the polymer segments is beyond a critical value. Spinodal-decomposition kinetics is predicted to occur during the ordering process. Thus the evolution of the density fluctuations during the induction period for PET and PEEK is consistent with these predictions. In the case of *i*-PP ($M_w = 520\,000$ g/mol, $M_w/M_n = 4.44$), our results suggest that the evolution of density fluctuations during the induction period can be attributed to effects arising from tacticity and a broad distribution in chain length. The PET, PEEK samples were also polydisperse ($M_w/M_n \geqslant 2.0$). Our latest studies[18] on a broad molecular-weight distribution linear polyethylene show that density fluctuations can be evident before crystal growth is evident in WAXS at low to moderate undercoolings. Our result, to be submitted later, can be interpreted to indicate that for all polymers, effects due to a broad distribution in chain length can determine whether one observes density fluctuations during the induction period.

The objective of this paper is to study the nature of density fluctuations during the period preceding lamellar crystal growth and the evolution of the fluctuations to lamellar crystals and supramolecular structures for a linear polyethylene fraction ($M_w = 32\,100$ g/mol, $M_w/M_n = 1.1$)[23] by simultaneous real time SAXS and WAXS measurements at a synchrotron source. The crystal growth kinetics of this sample has been previously studied[4] at 127.5 °C, which corresponds to an undercooling of 16.5 °C, by simultaneous SAXS and WAXS with synchrotron radiation. By comparing the crystallinity from WAXS and total scattering from SAXS, the authors were able to separate primary and secondary crystallization. They suggested that secondary crystallization takes place within the lamellar stacks where crystals become thicker and the amorphous layers become thinner. This conclusion was based on the observation of a constant SAXS peak position while the crystallinity increased during secondary crystallization. In that study only one SAXS peak was observed. On the other hand, in other studies on SRM 1483[19,20] and other polyethylenes,[19–22] two peaks in the SAXS profile have been observed when a sample is crystallized as will be shown. Our SAXS measurements also show two peaks and the positions of both SAXS peaks vary during crystallization at the temperatures studied.

In this paper, morphological quantities extracted from our SAXS and WAXS data are evaluated and compared with a model for the crystallizing system which accounts for the changes in the fraction of lamellar aggregates. We demonstrate that the variations in the SAXS profile can be correlated to the morphological changes associated with the evolution of isolated crystals to lamellar aggregates. We discuss the relative importance of two secondary crystallization processes, namely the formation of new lamellar stacks and increase in the crystallinity within lamellae, during and after primary crystallization.

II. EXPERIMENT

Measurements were performed on a linear polyethylene [standard reference material (SRM) 1483]. SRM 1483 (LPE) was prepared by a large-scale preparative gel permeation chromatography from a linear commercial polyethylene (SRM 1475). A more detailed description of the characterization procedures used has been given in the NIST certificate of analysis for SRM 1483. The number average molecular mass,[23] $M_n = 28\,900$ g/mol was determined by membrane osmometry in 1-chloronaphtalene at ~130 °C. The mass average molecular mass,[23] $M_w = 32\,100$ g/mol, was determined by light scattering in 1-chloronaphtalene at 135 °C. The polydispersity of the sample is 1.1. The equilibrium melting point of the sample is 144 °C.[24]

For x-ray measurements, samples were melt pressed in a vacuum laboratory hot press (Carver press, Model C)[25] at 160 °C for 30 min at 13 345 N. The molded films were then allowed to cool to room temperature under vacuum. A dual temperature chamber jump unit used for the melt crystallization experiments consists of two large thermal chambers maintained at the melt temperature ($T_1 = 160$ °C, 5 min) and a crystallization temperature (T_2). The copper sample cell was transferred rapidly (≈2 s) from one chamber (T_1) to the other (T_2) by means of a metal rod connected to a pneumatic pressure device. A detailed description of the arrangement of the sample and of the two detectors used to measure WAXS and SAXS simultaneously has been provided previously.[26,27] Each polymer sample within the copper cell was 1.5 mm thick and 7 mm in diameter and was contained between two 25 μm-thick Kapton films. The actual sample temperature during crystallization and melting was monitored by means of a thermocouple inserted into the sample cell. The crystallization temperatures studied (127 °C, 128 °C, and 129 °C) were usually reached without overshooting, 120 s after transfer. Under isothermal conditions the fluctuations in the sample temperature are less than 0.2 °C. Unless stated otherwise, all references to time are times elapsed after transferring the sample to the crystallization chamber.

Time-resolved simultaneous SAXS–WAXS data were collected at the advanced polymer beamline at Brookhaven National Laboratory, X27C. The radiation spectrum from the source was monochromated using a double multilayer monochromator and collimated with three 2° tapered tantalum pinholes to give an intense x-ray beam at $\lambda = 1.307$ Å.[26] Two linear position sensitive detectors (European Molecular Biology Laboratory, EMBL) were used to collect the SAXS and WAXS data simultaneously. For SAXS, the detector was located 1940 mm from the sample position. A vacuum chamber was placed between the sample and both detectors to reduce air scattering and absorption. The usable span of scattering vector magnitudes [$q = (4\pi/\lambda)\sin(\theta)$ and 2θ is the scattering angle] for SAXS was in the range $0.01\,\text{Å}^{-1} < q < 0.3\,\text{Å}^{-1}$ while that for WAXS was $0.5\,\text{Å}^{-1} < q < 2.6\,\text{Å}^{-1}$. Scattering patterns from silver behenate and Lupolen were used for angular calibration of the SAXS detector. NIST standards SRM 674A (α-Al_2O_3) and SRM 675 (Mica), and Lupolen were used for angular calibration of the WAXS detector. A parallel plate ionizing detector placed before the sample cell was used to record the incident inten-

sities. The experimental intensities were corrected for background scattering from the camera, temperature chamber and empty cell, incident intensity variations, and pixel-by-pixel detector sensitivity. The latter was established from the scattering of an Fe source. Two data acquisition times of 15 and 30 s were used depending on the crystallization rate.

The degree of crystallinity can be obtained by assuming that the total scattering in reciprocal space is independent of the state of aggregation of the polymer. The degree of crystallinity (mass fraction, w_c) may be found from $w_c = I_c / I_t$. The total scattering $I_t = I_c + I_a$. The amorphous and crystalline contributions to the total scattering are I_c and I_a, respectively. The combined area (I_t) under the 110 and 200 crystalline reflections was obtained by integrating the Lorentz corrected intensity ($I(q)q^2$) in the range $1.45\,\text{Å}^{-1} < q < 1.72\,\text{Å}^{-1}$. At temperatures above the melting temperature ($T \gg T_m$) of the sample the integrated intensity in the range $1.45\,\text{Å}^{-1} < q < 1.72\,\text{Å}^{-1}$ gives the value of I_a and the value at the crystallization temperature ($T = T_c$) gives I_t allowing I_c to be calculated.

The uncertainty in w_c by this method is about 2%. At low crystallinities ($w_c < 5\%$), it is difficult to determine the crystallinity of the sample within reasonable limits of uncertainty when numerical methods are applied to resolve the crystalline peaks from the amorphous background. The uncertainties associated with the values obtained overshadow changes that can be observed when the crystallinity is low.

The peak position, peak height and peak width for the crystalline and amorphous reflections in WAXS were extracted by a curve fitting program. A broad Gaussian peak was used to describe the amorphous background. The crystalline peaks (110 and 200) were also fitted with Gaussian functions. The peak positions of (110) and (200) were used to determine the unit cell lattice parameters of *a* and *b*.

The scattering intensity due to thermal fluctuations (I_b) was subtracted from the SAXS profile $I(q)$ by evaluating the slope of $I(q)q^4$ versus q^4 plots[28] at large wave vectors ($q \gg 0.2\,\text{Å}^{-1}$). This subtraction has to be done before any quantities are calculated from the SAXS profile. The small-angle scattering invariant is a measure of the total small-angle scattering from a material, independent of the size or shape of the structural inhomogeneities.[29] The absolute value of the invariant requires absolute intensity measurements, thermal background subtraction and extrapolation to $q = 0$ and $q = \infty$. However, the major contribution to the experimental invariant can be used to characterize structure development. Therefore, we calculate a relative SAXS invariant, Q_{SAXS}, from the area under the $(I(q) - I_b)q^2$ versus q curve between the first reliable data point at $q = 0.01$ to $0.2\ \text{Å}^{-1}$, beyond which $(I(q) - I_b)q^2$ remains constant. Long periods, are determined by applying Bragg's law to the peak positions of the Iq^2 versus q curve. The long period represents the periodicity of the sum of the crystalline and noncrystalline thicknesses.

III. MODEL

The SAXS invariant for a system where all the crystallizable units are within supermolecular structures is given by[30]

$$Q_{\text{SAXS}} = C x_s x_L x_{\text{CL}} (1 - x_{\text{CL}}) (\Delta\rho)^2. \tag{1}$$

In Eq. (1), C is a factor dependent on geometry and other quantities kept constant during the experiment, $\Delta\rho$ is the electron density difference between the crystalline and amorphous phases, x_s is the volume fraction of polymer transformed into supermolecular structure, x_L is the volume fraction of lamellar stacks within the superstructures and x_{CL} is the fraction of crystals within the lamellar stacks. The implicit assumption of this model is that all the crystals are in lamellar stacks and there are only two phases (crystalline and amorphous). In addition, the fraction $1 - x_s$, which is not involved in forming the supermolecular structures, does not contribute to Q_{SAXS}.[30]

The crystallinity index measured by WAXS (w_c) is the total mass fraction of crystals within the sample which is related to the above quantities by

$$w_c = \left(\frac{\rho_c}{\rho_s}\right) \Phi_c, \tag{2}$$

$$\Phi_c = x_s x_L x_{\text{CL}}, \tag{3}$$

$$\rho_s = \rho_c \Phi_c + \rho_a (1 - \Phi_c), \tag{4}$$

where Φ_c is the volume fraction crystallinity which can be estimated from WAXS. The electron densities of the crystalline and amorphous regions are designated by ρ_c and ρ_a and that of the sample is ρ_s. The factor (ρ_c / ρ_s) is included to convert volume fractions to mass fractions.

According to this model, x_s increases from 0 to 1 during primary crystallization. During the primary crystallization of most polymers, the change of x_{CL} is small as compared to the variation in $x_s x_L$ so that x_{CL} can be considered to be almost constant. As a result, Q_{SAXS} and w_c or Φ_c are proportional to $x_s x_L$ [Eqs. (1) and (3)]. This will also be the case if spherulitic growth occurs rapidly and the fraction of lamellar stacks within the spherulite continues to increase while x_{CL} remains constant. In contrast, during secondary crystallization involving only an increase in x_{CL} with x_L and x_s constant, Q_{SAXS} is proportional to $x_{\text{CL}}(1 - x_{\text{CL}})$ while w_c is proportional to x_{CL}. Thus, for this model during secondary crystallization, the change in w_c will be larger than the change of Q_{SAXS}, while during primary crystallization Q_{SAXS} and w_c are proportional to each other.

IV. RESULTS AND DISCUSSION

A. Induction period

As a polymer melt is transformed to the crystalline state, one expects the peak intensity of the amorphous scattering to decrease while that of the crystalline reflections increase. As lamellar sheaves are developed, a simultaneous increase in the SAXS peak intensity is expected. Figures 1–3 show the change of the SAXS and WAXS intensity profiles during the early stage isothermal crystallization of LPE at 127 °C, 128 °C, and 129 °C after melting at 160 °C for 5 min. The time dependence of the peak intensity of the amorphous scattering is shown in Fig. 4. At the temperatures studied, when changes in the SAXS intensity profile at low wave vectors and the area under the crystalline reflections are observed

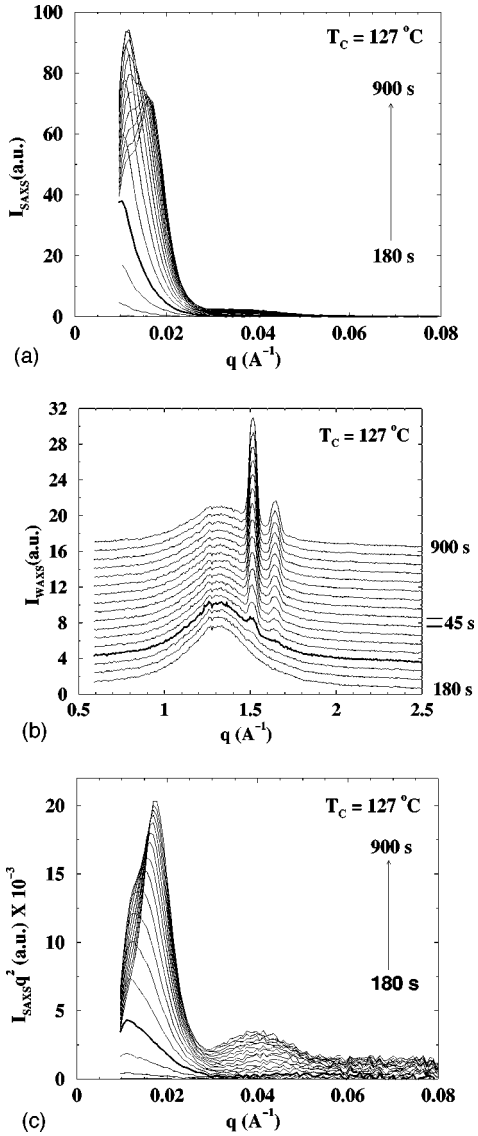

FIG. 1. Development of typical SAXS and WAXS during isothermal crystallization of the sample SRM 1483 (M_w=32 100) at 127 °C within the first 900 s after melting at 160 °C for 5 min; (a) SAXS, intensity I_{SAXS}; (b) WAXS, intensity I_{WAXS}; (c) SAXS, intensity $I_{SAXS}q^2$. SAXS intensity represents excess scattering due to density fluctuations at the crystallization temperature since melt has been subtracted. The relative standard deviation in the SAXS intensity values in the range 0.01 Å^{-1} $<q<$ 0.02 Å^{-1} is less than 2%. At higher wave vectors, the relative standard deviation increases with q and the maximum value is less than 15%. Bold curves denote the end of Stage I. WAXS curves have been offset for clarity.

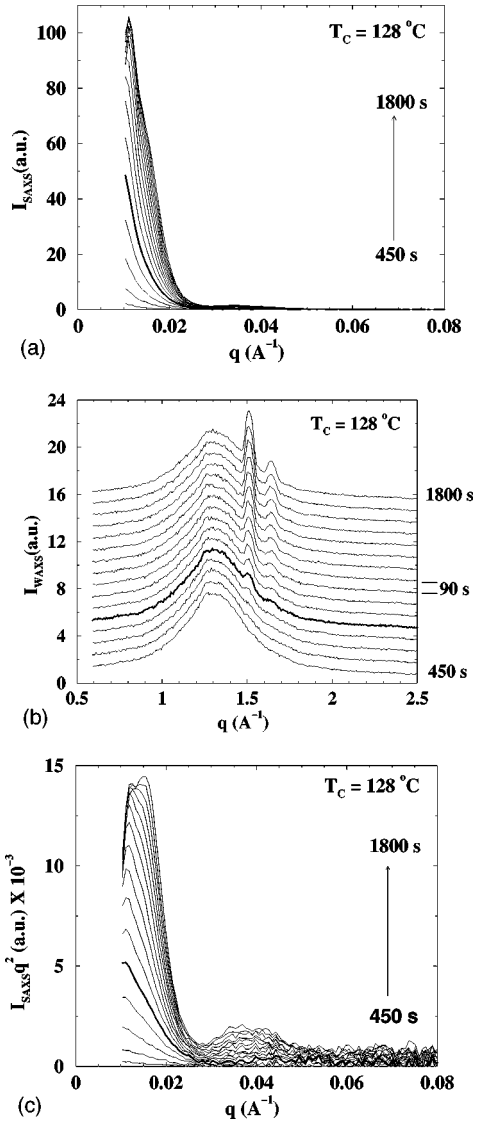

FIG. 2. Development of typical SAXS and WAXS during isothermal crystallization of the sample SRM 1483 (M_w=32 100) at 128 °C within the first 1800 s after melting at 160 °C for 5 min; (a) SAXS, intensity I_{SAXS}; (b) WAXS, intensity I_{WAXS}; (c) SAXS, intensity $I_{SAXS}q^2$. SAXS intensity represents excess scattering due to density fluctuations at the crystallization temperature since melt has been subtracted. The relative standard deviation in the SAXS intensity values in the range 0.01 Å^{-1} $<q<$ 0.02 Å^{-1} is less than 2%. At higher wave vectors, the relative standard deviation increases with q and the maximum value is less than 15%. Bold curves denote the end of Stage I. WAXS curves have been offset for clarity.

(Figs. 1–3), the peak intensity of the amorphous scattering starts to decrease (Fig. 4). Moreover, at higher temperatures than 129 °C, changes in the SAXS and WAXS scattering profiles also occurred simultaneously even when the samples were observed for several hours before these changes occurred.

At each temperature, there is a characteristic time (induction time), associated with the time to form crystals from the amorphous state. This time increases with crystallization temperature. During the induction period, we are unable to resolve any changes in the SAXS and WAXS scattering profiles. One possible explanation for our observations is that if local ordering occurs everywhere in the sample and the resulting regions are uncorrelated spatially, and since the density contrast between the dense and less dense regions is very small, no intensity variations in SAXS will be observed. In WAXS, Bragg peaks will be observed for nuclei that possess three dimensional order and a concentration above a threshold for detection. If, however, spinodal decomposition plays a major role in the nucleation of crystals, development of a SAXS pattern due to density fluctuations should occur prior to any WAXS from crystals because there is a continuous transformation of the partially ordered phase through slightly more ordered states.[32] The characteristic length scale associated with the developing spinodal texture gives rise to a SAXS peak. Initially, the SAXS peak intensity grows expo-

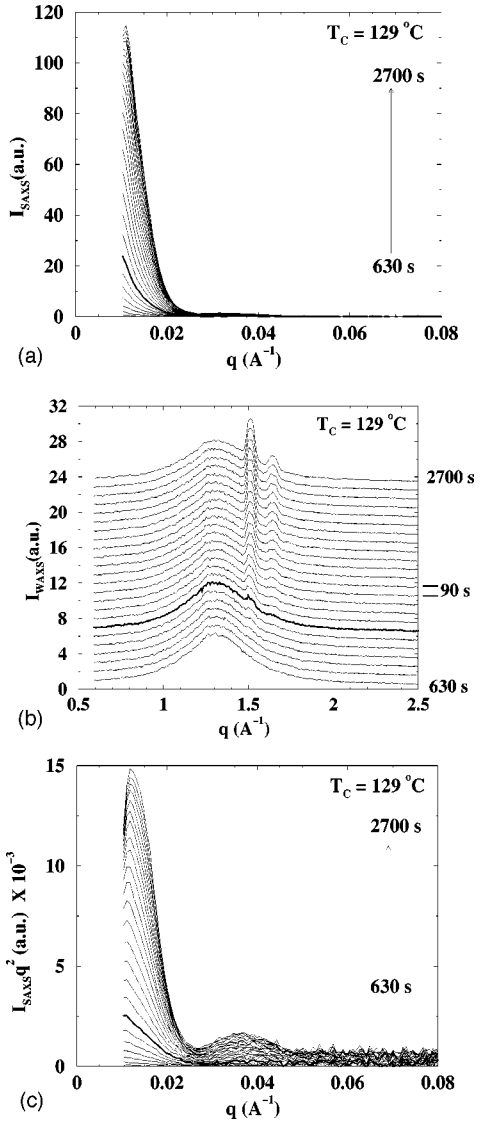

FIG. 3. Development of typical SAXS and WAXS during isothermal crystallization of the sample SRM 1483 (M_w=32 100) at 129 °C within the first 2700 s after melting at 160 °C for 5 min; (a) SAXS, intensity I_{SAXS}; (b) WAXS, intensity I_{WAXS}; (c) SAXS, intensity $I_{SAXS}q^2$. SAXS intensity represents excess scattering due to density fluctuations at the crystallization temperature since melt has been subtracted. The relative standard deviation in the SAXS intensity values in the range $0.01\ \text{Å}^{-1} < q < 0.02\ \text{Å}^{-1}$ is less than 2%. At higher wave vectors, the relative standard deviation increases with q and the maximum value is less than 15%. Bold curves denote the end of Stage I. WAXS curves have been offset for clarity.

nentially with time while the corresponding peak position remains constant. As these domains coarsen, the peak position shifts to small wave vectors and further growth is arrested once Bragg peaks appear in the WAXS intensity profile. Since we observe no changes in the SAXS profile before changes are observed in the WAXS scattering, our results indicate that the mechanism for initiating crystallization is inconsistent with spinodal dynamics but instead can best be described by nucleation followed by growth.

B. Evolution of crystal morphology

For the sample studied, superstructures such as spherulites (formed below 127 °C) and axialites (formed above

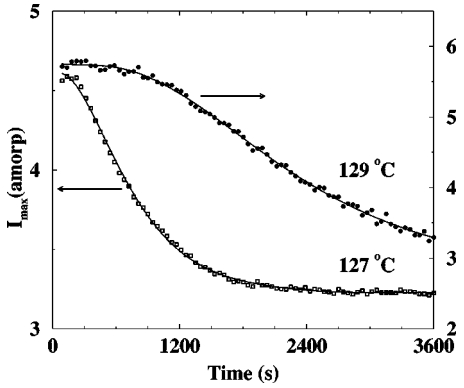

FIG. 4. Peak intensity of the amorphous halo during crystallization of LPE at 127 °C and 129 °C. The relative standard deviation associated with estimating the amorphous peak values is about 1%.

127 °C) consisting of crystalline and noncrystalline regions grow during crystallization from the melt.[3,31,33] Lateral habits characteristic of the constituent lamellae in spherulites and axialites have been identified and extensively studied[33–35] by electron microscopy. Toda[33] showed that single crystals could be observed during the early stage of crystallization for linear polyethylene fractions (SRM 1482 and SRM 1483) and these crystals evolve into multilayer aggregates at later times. Solution cast thin films were isothermally crystallized from the melt and quenched in acetone at 0 °C or −80 °C. Single crystals were obtained by using the extraction technique of Basset *et al.*[36] and observed under the electron microscope. At the temperatures studied in the present investigation, the observed changes in the SAXS and WAXS scattering profiles can be divided into three distinctive stages which reflect the evolution of isolated crystals to lamellar aggregates as suggested by the microscopic observations of Toda.[33]

During Stage I, the SAXS intensity at $q < 0.02\ \text{Å}^{-1}$ increases while that at higher wave vectors remained constant. Meanwhile the apparent crystallinity from WAXS increases to about 10% before two peaks could be resolved in the SAXS intensity profile. The first SAXS peak will be referred to as P_1 and the second as P_2 in subsequent discussion. Bold curves in Figs. 1–3 indicate the end of Stage I. As lamellar stacks are developed in Stage II, the period corresponding to the first SAXS peak (L_1) decreases (Figs. 5 and 6). On the other hand, the period corresponding to the second SAXS peak (L_2) progressively increases with crystallization time (Figs. 5 and 6). Finally, during Stage III, the crystallinity and L_2 further increases (Figs. 5 and 6). L_1 increases after reaching a minimum value and the invariant becomes constant.

According to Eqs. (1) and (3), if one assumes that during the growth of superstructures (primary crystallization), the variation in x_{CL} is small as compared to the change in $x_s x_L$ such that x_{CL} can be considered to be almost constant, Q_{SAXS} and w_c should change proportionally to one another. We observe this variation during Stages I and II (Figs. 5 and 6). In this case, primary crystallization ends when the fraction of crystalline material transformed $[X(t)=w_c(t)/w_c(t=\infty)]$ is between 80% and 95%, i.e., 750 to 1050 s at 127 °C and 2100 to 2700 s at 128 °C (Figs. 5 and 6). These values are

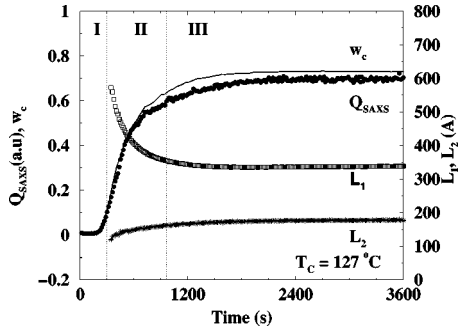

FIG. 5. Changes in morphological quantities for synchrotron SAXS–WAXS during crystallization of LPE at 127 °C: Degree of crystallinity determined from WAXS w_c (—), SAXS invariant Q_{SAXS} (●), the period corresponding to the first SAXS peak (L_1) and the period corresponding to the second SAXS peak (L_2) obtained from Iq^2 curve. The uncertainty in w_c is about 2%. The relative standard deviation associated with estimating L_1 and L_2 is less than 1%.

consistent with the crystallinity that develops after primary crystallization by other methods such as DSC.

From an Avrami[37] analysis of DSC crystallization isotherms, a break in the time dependence of the crystallization isotherms is observed. The significance of this break has been attributed to the continuation of secondary processes which dominate at the end of the primary crystallization.[38] From these studies, over 90% of the crystallinity develops during primary crystallization. The end of primary crystallization is usually estimated as twice the half time of crystallization.[4] The end of primary crystallization estimated by the DSC method corresponds to the dotted line showing the end of Stage II in Figs. 5 and 6. It is within the range that one would predict on the basis of the variation in Q_{SAXS} and w_c.

In order to characterize the secondary mechanisms during and after primary crystallization, the changes in morphological quantities extracted from our SAXS and WAXS data are discussed below and compared to predictions based on Eqs. (1)–(4). During the initial increase in the SAXS intensity at low q in Stage I, there is no second peak in the SAXS profile. The absence of this peak may be due to a small

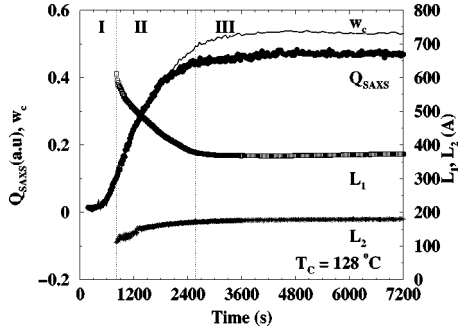

FIG. 6. Changes in morphological quantities for synchrotron SAXS–WAXS during crystallization of LPE at 128 °C: Degree of crystallinity determined from WAXS w_c (—), SAXS invariant Q_{SAXS} (●), the period corresponding to the first SAXS peak (L_1) and the period corresponding to the second SAXS peak (L_2) obtained from Iq^2 curve. The uncertainty in w_c is about 2%. The relative standard deviation associated with estimating L_1 and L_2 is less than 1%.

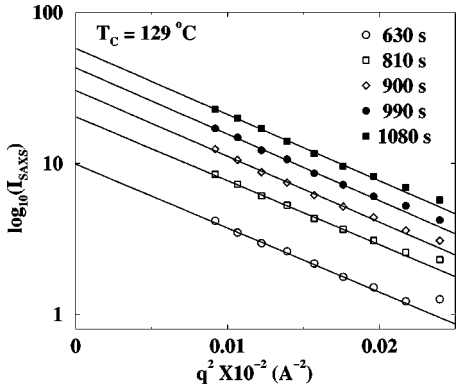

FIG. 7. Guinier plots for various crystallization times in Stage I. Lines represent fits to the data points using Eq. (5).

population of lamellar stacks (small x_L) or monolayer lamellar crystals.[39,40] In order to distinguish between these two cases we apply Guinier's analysis for an isolated domain system at very high dilution and for a randomly oriented thin platelets to the period in Stage I where a second SAXS peak cannot be resolved. The intensity variations are given by[41]

$$I(q,t) \propto \exp\left[-\frac{R_g^2 q^2}{3}\right], \tag{5}$$

$$I(q,t) \propto q^{-2} \exp\left[-\frac{l_g^2 q^2}{12}\right], \tag{6}$$

where R_g is the radius of gyration of the isolated domain and l_g is the thickness of the platelet. Figure 7 shows typical Guinier plots of the data using Eq. 5 showing good agreement with the equation. In Fig. 8, the radius of gyration of the isolated domain is shown as a function of crystallization time at 129 °C. At this temperature, a dense domain with an R_g of 173 Å is formed initially. The average size of this domain does not change (Fig. 8). Similar results are obtained for the platelet thickness and at lower temperatures (Table I).

The kinetic theories of Hoffman *et al.*[3] predict that the initial lamellar thickness formed (l^*) is given by

$$l^* = \frac{2\sigma_e T_m^o}{\Delta h_f \Delta T} + \delta l, \tag{7}$$

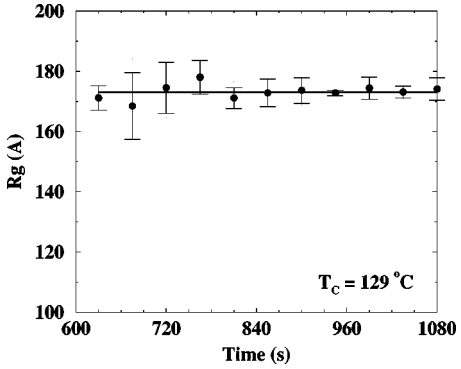

FIG. 8. Time variation of the radius of gyration (R_g) of the isolated domain in Stage I. Error bars are the standard deviation in the estimation of R_g from the fit of the data in Fig. 7 to Eq. (5).

TABLE I. Domain sizes during Stage I: Radius of gyration of isolated domains at high dilution (R_g); Thickness of randomly oriented thin platelets (l_g); Range of crystal thickness predicted by the secondary nucleation (l^*); Measured values of the initial crystal thickness l_m^*. The l^* values reflect a range spanning the theoretical value of δl and the maximum value from experiments. The ± values denote the standard deviation.

Temperature (°C)	R_g (Å)	l_g (Å)	l^* (Å)	l_m^*
127	(162±7) Å	(169±22) Å	168 Å–217 Å	200 Å
128	(171±7) Å	(194±14) Å	178 Å–227 Å	220 Å
129	(173±5) Å	(195±15) Å	189 Å–238 Å	···

where the quantity Δh_f is the heat of fusion, the equilibrium melting point is T_m^o and $\Delta T = T_m^o - T_c$. The theory predicts a δl value of 10–15 Å. Experiments carried out on solution and melt crystallized polyethylene under conditions where lamellar thickening is not observed yield an average value $\delta l = 43$ Å; $\delta l_{\min} = 28.1$ Å and $\delta l_{\max} = 58.7$ Å.[42–44] By substituting of values appropriate to SRM 1483 crystallized from the melt[24] ($\Delta h_f = 280\ \mathrm{J\,cm^{-3}}$, $T_m^o = 417$ K, and $\sigma_e = 90\ \mathrm{mJ\,m^3}$) and accounting for the variation in δl, l^* is found to range from 168 to 238 Å for the temperatures studied (Table I). The Guinier plot, interpreted in terms of scattering by monolayer lamellar crystals, should give a domain size similar to that found for the crystal thickness at the same temperature. There is good agreement between the size of the platelet thickness and measured lamellar thickness at each temperature, hence the scattering can be attributed to individual lamellar crystals. In the view of our model, Q_{SAXS} and w_c increase proportionally as the fraction of material within the superstructures increases with x_{CL} relatively constant. This interpretation is consistent with crystal growth without lamellar thickening, i.e., no increases in x_{CL}. In effect, crystal growth occurs at *constant crystal thickness* during Stage I.

The individual lamellar scattering evident in Stage I can be interpreted in terms of a skeletal spherulite model, wherein lamellar ribbons extend as units or complete groups outward into the melt.[39] For the crystallization temperatures studied, one sees that the scattering intensity at $q < 0.2\ \mathrm{Å^{-1}}$ diminishes as the crystallization time is increased [Figs. 1(a), 2(a), and 3(a)] in Stage II. It has been shown previously[39,40] that the decrease in the scattering at low angles during crystallization is associated with growth of new crystallites within the amorphous gaps in the lamellar stacking within spherulites.

In Stage II, Q_{SAXS} and w_c vary proportionally to one another while the intensity of the SAXS peaks increases (Fig. 9). These changes would occur if the growth of the superstructures occurs rapidly and the fraction of lamellar stacks within the superstructures continues to increase while x_{CL} is relatively constant. In this case, the secondary process involving the creation of new stacks (increase in x_L) is more important than processes that initially results in an increase in the crystallinity (increase in x_{CL}) within the stacks (Figs. 5 and 6). During the latter parts of Stage II, Q_{SAXS} and w_c vary differently with crystallization time. This would occur if processes that increase x_{CL} become more important than the increase in the number of stacks. In effect, the $x_{\mathrm{CL}}(1-x_{\mathrm{CL}})$ contribution to Q_{SAXS} dominates the variation of $x_s x_L$ during the latter stages of primary crystallization. In Stage III, further increases in Q_{SAXS} and w_c are mainly due to increases in x_{CL} even though the concentration of lamellar stacks may continue to increase.

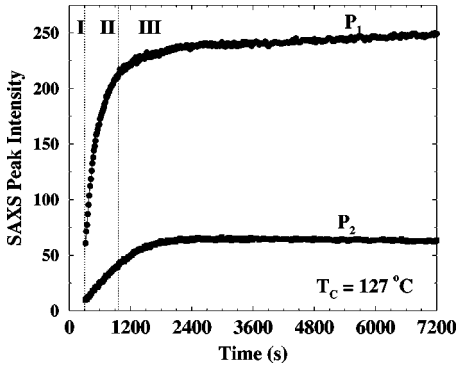

FIG. 9. SAXS peak intensities determined from the Iq^2 curve during crystallization of LPE at 127 °C.

The growth of new crystallites are discussed below with reference to data obtained at 127 °C. Similar processes are observed at higher temperatures. At the beginning of Stage II, L_1 is much larger than $2L_2$, suggesting that L_2 is not a second order reflection of L_1 (Figs. 5 and 6). From Table I the size of the crystallites during Stage I is about 200 Å (Table I). If L_1 represents the average distance between the isolated crystals in Stage I then these crystals are separated by amorphous regions that are about two times the crystal size at the beginning of Stage II. Hence the decrease in L_1 during Stage II can then be attributed to the growth of new lamellae in the amorphous regions surrounding existing lamellae. The continuous increase in the peak intensity of P_1 indicates that the number of repeat units (one crystalline plus one amorphous layer) is increasing (Fig. 9). Perfection of periodicity within stacks can also account for the initial part of the increase since the width of the first SAXS peak decreases rapidly during Stage II and stays constant in Stage III. The width of P_2 is relatively constant during both stages.

The relative intensities of the various orders of Bragg maxima are controlled by the structure factor of the repeat unit and by the perfection of the periodicity. As the number of repeat units and perfection in stacking increase, the relative intensity of the higher order maxima should increase. By the end of Stage II, L_1 is about 355 Å (Table II). If there is a high degree of ordering within the lamellar stacks, a second order peak near 177.5 Å would be observed. The increase in intensity in the vicinity of the apparent second order peak

TABLE II. SAXS peak parameters during crystallization: Period of the first SAXS peak after 3 h (L_1^*); Period of the second SAXS peak after 3 h (L_2^*); Value of L_1 at its minimum ($L_1^{\min}$). The time corresponding to $L_1^{\min}$ is $t_{\min}$. The uncertainty associated with estimating the long periods is about 1 Å.

Temperature (°C)	L_1^* (Å)	L_2^* (Å)	$L_1^{\min}$	$t_{\min}$ (s)
127	343 Å	180 Å	335 Å	1920 s
128	373 Å	180 Å	367 Å	4050 s
129	454 Å	185 Å	454 Å	7020 s

(P_2) is consistent with increases in the number of repeat units and perfection in stacks with a long period L_1. However, if P_2 was only a second order reflection of P_1 then the widths of the peaks should be the same. In Stage III, the width of P_1 does not change and the width of P_2 is about 2.6 times P_1. This reflects the superposition of a second periodicity or a distribution of periodicities upon the second-order reflection of the first SAXS peak. In order to raise the apparent second-order peak intensity, the other periods must be somewhere near half the major period (L_1). This is the period that would be expected for crystals that fill in the amorphous regions between existing lamellar stacks. Thus even though at long times L_1 will be close to $2L_2$, the two peaks do not represent one periodicity but a broad distribution of lamellar thicknesses. A broad distribution in lamellar thickness is expected from the standpoint of the thickening of lamellae once they are formed. This existence of a broad distribution of lamellar thicknesses implies that the evolution of the first and second SAXS peaks will be different.

Previous electron microscopic studies[45–48] of various linear polyethylenes with broad and narrow molecular mass distributions crystallized from the melt have shown that fractionation during crystal growth tends to place different molecular lengths in specific regions within the spherulites. In general, two types of lamellae, namely dominant and subsidiary, may be distinguished. Dominant lamellae refer to the first-formed and thicker lamellae while thinner and later-forming lamellae located between dominant lamellae are termed subsidiary. For a linear polyethylene with $M_w = 31\,000$ g/mol with a polydispersity 1.3, dominant, subsidiary and lamellae which form on quenching are observed when the sample is crystallized at 130.4 °C for 27 *d* and quenched.[48] The quenched lamellae contain the shortest molecules. However, the difference in the dominant and subsidiary lamellae can be a consequence a number of reasons.

New, misaligned lamellae, can be formed from molecules remaining in the melt (surrounding the dominant lamellae) by nucleation on pre-existing crystals.[47] The dominant lamellae can create geometric confinements that preclude even polymers of the same chain length as those incorporated in the dominant stacks from forming the preferred secondary structure. Thinner lamellae that are formed in regions where the melt is restrained by the dominant lamellae can also be explained by a thermodynamic standpoint. In these regions, the entropy change on crystallization will be smaller than that associated with transforming a virgin melt to a crystal. As a result, the local equilibrium melting temperature will be raised, thereby reducing the critical lamellar thickness required to form a stable nucleus. As new crystals are formed by nucleation on pre-existing crystals or from a melt restrained by dominant lamellae, one would expect a decrease in the average crystal thickness or long period which is consistent with the observed decrease in L_1 during Stages II and III.

In Stage III at 127 °C, L_1 increases after reaching a minimum value of 335 Å at 1920 s. The time to observe a minimum in L_1 ($t_{\min}$) and the minimum value of L_1 increase strongly with temperature (Table III). In view of our observations, $t_{\min}$ could correspond to the time where the rate at which new stacks are formed goes to zero. Consequently, the intensity increase in P_1 after this minimum can be solely attributed to an increase in the crystallinity within the stacks (increase in x_{CL}). Increases in x_{CL} can be due to both thickening which reduces the amorphous content as well as ''internal'' improvements in stem packing.

TABLE III. Average values of the *a* and *b* unit cell lattice parameters during Stages II and III of crystallization of LPE at 127 °C, 128 °C, and 129 °C. The ± values denote the standard deviation.

Temperature (°C)	*a* (Å)	*b* (Å)
127	(7.634±0.002) Å	(4.937±0.002) Å
128	(7.644±0.003) Å	(4.945±0.002) Å
129	(7.640±0.004) Å	(4.945±0.002) Å

A detailed analysis of our synchrotron WAXS data show that the *a* and *b* unit cell lattice parameters remain unchanged during Stages II and III (Table III). For orthorhombic polyethylene, the *a* and *b* parameters at room temperature are 7.417 and 4.945 Å.[49] At higher temperatures, thermal expansion accounts for deviations of these values with the *a* axis more sensitive to temperature than the *b* axis (Table III). In contrast, the full-width at half maximum (FWHM) of 110 and 200 reflections observed at 127 °C, decreases during Stage II while a negligible change is observed for the FWHM of the 110 reflection at 128 and 129 °C [Figs. 10(b) and 10(c)]. The full-width at half maximum is a measure of broadening of the crystalline peaks due to finite crystal size and imperfections within the crystal. In the absence of higher order reflections one cannot conclusively say which of these contributions to this quantity is dominant. The decreases in the FWHM observed in Stage II do indicate that crystal perfection occurs during the growth of the crystalline phase and reflect improvements in lateral stem packing within lamellae.

The possibility that thickening of lamellar crystallites occurs during crystallization has been long established.[21,22,50–54] However there has been little agreement concerning the mechanism of the thickening process. Hoffman and Weeks[22] suggested that the thickening process can be described by an empirical relationship where the long period increases logarithmically with time. They chose the second SAXS peak we observe to represent the long period. Both of these groups identified two regions of thickening. An initial rapid thickening is followed by a slower rate of thickening. An early comprehensive study[51] employing longitudinal acoustic Raman modes, room temperature SAXS, and electron microscopy showed that molecular segregation coupled with isothermal thickening of initially formed lamellae are responsible for the period of initial rapid thickening. The continued thickening after crystallization is complete is caused by chain refolding alone.[51]

Our SAXS measurements show that the major long period (L_1) decreases, goes through a minimum and then increases at a protracted rate. We observe the largest changes in the major and minor long periods occur during primary crystallization once lamellar stacks are manifest in the SAXS profile. This large change is to be expected if, as material is incorporated into the growing crystal, reorganization of the

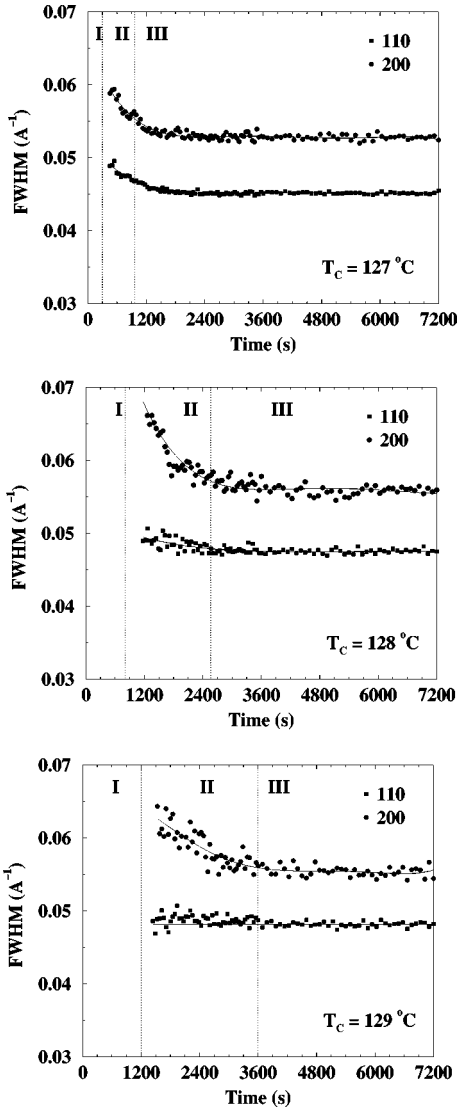

FIG. 10. Full width at half maximum (FWHM) of the 110 (■) and 200 (●) crystalline reflections (a) 127 °C, (b) 128 °C, and (c) 129 °C.

previously added material increases the crystalline fraction and perfection in the lateral packing of stems as suggested by WAXS. In fact, this process should occur most rapidly behind the growth front when lamellae are still surrounded by molten material. Thus the variations in L_1 and L_2 during Stages II and III, can be a consequence of a decreasing rate in the creation of new lamellar stacks and thickening of existing stacks.

In the synchrotron studies by Bark *et al.*[4] on a sample identical to the one used in this work, only one peak Bragg peak in the SAXS profile was resolved and this peak corresponds to P_2. The period corresponding to this peak remains constant while the crystallinity increases during secondary crystallization. On the basis of observations by Bark *et al.*[4], secondary crystallization was assumed to take place within the lamellar stacks where the crystals become thicker and the amorphous layers become thinner. Our results indicate that crystal thickening can occur once Bragg peaks are resolved in the SAXS intensity profile (Stages II and III). For crystallization near 127.5 °C, a period of 180 Å was obtained by Bark *et al.*[4] which is in good agreement with our limiting values at the temperatures studied (Table II).

Large variations in the average distance between two adjacent crystals was suggested by the broad SAXS peak in their measurements as is the case in our L_2 [Figs. 1(c), 2(c), and 3(c)]. A broad SAXS peak can arise if lamellae of different thicknesses are mixed or if there is a large variation in the distance between equivalent lamellae. We have indicated previously that the wide secondary SAXS peak (P_2) can result from a distribution of periodicities. Thus, even though on the size scale of several microns, one can identify different lamellar stacks by microscopy, our SAXS measurements indicate that there is a wide variation in distance between crystals within the subsidiary stacks since the width of P_2 is much larger than that for P_1. If one takes into account a wide variation in the distance between crystals, then there are two possible ways by which the concentration of lamellae may increase in Stage III (where our morphological model predicts that the observed increases in Q_{SAXS} and w_c are mainly due to increases x_{CL}). New lamellae (subsidiary lamellae) can be formed such that the ratio of the crystal/amorphous thicknesses does not change L_2 significantly. Alternatively, a decrease in the long period that one would anticipate as thinner lamellae are formed may not be sufficient to overcome an increase in average repeat distance of the crystals as existing crystals thicken (increase in x_{CL}).

V. CONCLUSIONS

The simultaneous measurement of SAXS and WAXS for a narrow-molecular mass distribution polyethylene demonstrates that the mechanism for initiating crystallization is nucleation followed by growth as distinct from spinodal dynamics. The growth of these crystals can be described by a model where all the crystallizable units are within developing supermolecular structures. We have shown that local order develops first, followed by a subsequent increase in global order as lamellar stacks develop. We have demonstrated by SAXS that the two Bragg peaks usually observed for polyethylene represent a broad distribution in lamellar thickness. We have examined the relative importance of two secondary crystallization processes, namely the formation of new lamellar stacks and increase in the crystallinity within lamellar aggregates during and after primary crystallization. During the initial stages of primary crystallization, our results indicate that the crystallinity increases while average crystallite thickness remains constant. As lamellar stacks are developed, both secondary processes occur rapidly during primary crystallization where aggregates are still surrounded by molten material. However, when the rate of formation of new crystallites becomes negligible at long times, global crystalline order is attained by increasing the crystallinity within the lamellar stacks.

ACKNOWLEDGMENTS

Synchrotron work was carried out at the Advanced Polymer Beamline at the National Synchrotron Light Source, Brookhaven National Laboratory. We would like to thank Dr. C. Guttman for providing generous quantities of the

polymer studied and Dr. Freddy Khoury for his many helpful suggestions and discussions. We acknowledge helpful discussions with Dr. Benjamin Hsiao, Dr. Ty Prosa, Dr. Kalman Migler, and Dr. Jack Douglas. We would like to thank Feng-ji Yeh and Dr. Lizhi Liu for help with the x-ray setup.

[1] D. C. Bassett, *Principles of Polymer Morphology* (Cambridge University Press, Cambridge, 1981).
[2] P. H. Geil, *Polymer Single Crystals* (Wiley Interscience, Chichester, 1963).
[3] J. D. Hoffman, G. T. Davis, and J. I. Lauritzen, in *Treatise on Solid State Chemistry, Vol. 3, Crystalline and Noncrystalline Solids*, edited by N. B. Hannay (Plenum, New York, 1976), Chap. 7.
[4] M. Bark, H. G. Zachmann, R. Alamo, and L. Mandelkern, Makromol. Chem. **193**, 2363 (1992).
[5] H. H. Song, R. S. Stein, Q. D. Wu, M. Ree, J. C. Phillips, A. LeGrand, and B. Chu, Macromolecules **21**, 1180 (1988).
[6] H. H. Song, Q. D. Wu, B. Chu, M. Satkowski, M. Ree, R. S. Stein, and J. C. Phillips, Macromolecules **23**, 2380 (1990).
[7] J. Cronauer, Ph. D. Dissertation, ''*Undersuchung der Morphologie und Kristallisation von Polymeren und Polymermischungen unter Anwendung der gleichzeitigen Messung der Röntgenkleinwinkel-, Röntgenweitwinkel-, und Lichtstreuung*,'' University of Hamburg (Verlag Shaker, Hamburg, 1995).
[8] M. Imai, K. Kaji, and T. Kanaya, Phys. Rev. Lett. **71**, 4162 (1993).
[9] M. Imai, K. Mori, T. Mizukami, K. Kaji, and T. Kanaya, Polymer **33**, 4451 (1992).
[10] M. Imai, K. Kaji, and T. Kanaya, Macromolecules **27**, 7103 (1994).
[11] T. A. Ezquerra, E. López-Cabararcos, B. S. Hsiao, and F. J. Balta-Calleja, Phys. Rev. E **54**, 989 (1996).
[12] N. J. Terrill, P. A. Fairclough, E. Towns-Andrews, B. U. Koanschek, R. J. Young, and A. J. Ryan, Polymer **39**, 2381 (1998).
[13] J. W. Cahn and J. E. Hilliard, J. Chem. Phys. **28**, 258 (1958); J. W. Cahn, *ibid*. **42**, 93 (1965); H. E. Cook, Acta Metall. **18**, 297 (1970).
[14] P. D. Olmsted, W. C. K. Poon, T. C. B. McLeish, N. J. Terrill, and A. J. Ryan, Phys. Rev. Lett. **81**, 373 (1998).
[15] M. Doi, T. Shimada, and K. Okano, J. Chem. Phys. **88**, 2815 (1988).
[16] M. Doi, T. Shimada, and K. Okano, J. Chem. Phys. **88**, 4070 (1988).
[17] M. Doi, and S. F. Edwards, *The Theory of Polymer Dynamics* (Clarendon, Oxford, 1986).
[18] Yvonne A. Akpalu and Eric J. Amis (submitted).
[19] M. Peeters, B. Goderis, C. Vonk, H. Reynaers, and V. Mathot, J. Polym. Sci., Polym. Phys. Ed. **36**, 2689 (1997).
[20] M. Peeters, Ph.D. Dissertation, ''*Crystallization and Melting Behaviour of Homogeneous Copolymers of Ethene and 1-octene*,'' Katholieke Universiteit Leuven, June 1995.
[21] M. J. McCready and J. M. Schultz, J. Polym. Sci., Polym. Phys. Ed. **17**, 725 (1979).
[22] J. D. Hoffman and J. J. Weeks, J. Chem. Phys. **42**, 4301 (1965).
[23] According to ISO 31-8, the term ''Molecular Weight'' has been replaced by ''Relative Molecular Mass,'' symbol M_r. Thus, if this nomenclature and notation were to be followed in this publication, one would write $M_{r,n}$ instead of the historically conventional M_n for the number average molecular weight, with similar changes for M_w, M_z, and M_v, and it would be called the ''Number Average Relative Molecular Mass.'' The conventional notation, rather than the ISO notation, has been employed for this publication.
[24] J. D. Hoffman, Polymer **23**, 656 (1982).
[25] Certain equipment and instruments or materials are identified in the paper in order to adequately specify the experimental details. Such identification does not imply recommendation by the National Institute of Standards and Technology, nor does it imply the materials are necessarily the best available for the purpose.
[26] B. S. Hsiao, B. Chu, and F. Yeh, *NSLS Newsletter*, July, 1 (1997).
[27] B. S. Hsiao, K. H. Gardner, D. Q. Wu, and B. Chu, Polymer **34(19)**, 3996 (1993).
[28] J. J. Koberstein, B. Morra, and R. S. Stein, J. Appl. Crystallogr. **13**, 34 (1980).
[29] F. J. Balta-Calleja and C. G. Vonk, *X-ray Scattering of Synthetic Polymers* (Elsevier, London, 1989).
[30] C. Santa Cruz, N. Stribeck, H. G. Zachmann, and F. J. Balta-Calleja, Macromolecules **24**, 5980 (1991).
[31] J. D. Hoffman, L. J. Frolen, G. S. Ross, and J. I. Lauritzen, Jr., J. Res. Natl. Bur. Stand., Sect. A **79**, 671 (1975).
[32] G. Strobl, *The Physics of Polymers* (Springer, Berlin, 1996), p. 173.
[33] A. Toda, Colloid Polym. Sci. **270**, 667 (1992).
[34] A. Toda and A. Keller, Colloid Polym. Sci. **271**, 328 (1993).
[35] A. Toda, Faraday Discuss. **95**, 129 (1993).
[36] D. C. Bessett, R. H. Olley, and I. A. M. Al Raheil, Polymer **29**, 1539 (1988).
[37] M. J. Avrami, Chem. Phys. **7**, 1103 (1939); J. Chem. Phys. **9**, 177 (1941).
[38] J. N. Hay and P. J. Mills, Polymer **23**, 1380 (1982).
[39] J. M. Schultz, J. S. Lin, and R. W. Hendricks, J. Appl. Crystallogr. **11**, 551 (1978).
[40] J. M. Schultz, J. Polym. Sci., Polym. Phys. Ed. **14**, 2291 (1976).
[41] A. Guinier and G. Fournet, *Small-Angle Scattering of X-rays* (Wiley & Sons, London, 1955).
[42] P. J. Barham, R. A. Chivers, A. Kellar, J. Martinez-Salazar, and S. J. Organ, J. Mater. Sci. **20**, 1625 (1985).
[43] J. Martinez-Salazar, P. J. Barham, and A. Kellar, J. Mater. Sci. **20**, 1616 (1985).
[44] S. J. Organ and A. Kellar, J. Mater. Sci. **20**, 1602 (1985).
[45] D. C. Bassett and A. M. Hodge, Proc. R. Soc. London, Ser. A **377**, 25 (1981).
[46] D. C. Bassett and A. M. Hodge, Proc. R. Soc. London, Ser. A **377**, 39 (1981).
[47] D. C. Bassett and A. M. Hodge, Proc. R. Soc. London, Ser. A **377**, 61 (1981).
[48] D. C. Bassett, A. M. Hodge, and R. H. Olley, Discuss. Faraday Soc. **68**, 218 (1979).
[49] C. W. Bunn, Trans. Faraday Soc. **35**, 482 (1939); S. Kavesh and J. M. Schultz, J. Polym. Sci., Part A-2, **8**, 243 (1970).
[50] T. Kawai, Kolloid Z. Z. Polym. **229**, 116 (1969).
[51] J. Dlugosz, G. V. Fraser, D. Grubb, A. Keller, J. A. Odell, and P. L. Goggin, Polymer **17**, 471 (1976).
[52] G. M. Stack, L. Mandelkern, and I. G. Voight-Martin, Polym. Bull. (Berlin) **8**, 421 (1982).
[53] R. A. Chivers, P. J. Barham, J. Martinez-Slazar, and A. Keller, J. Polym. Sci., Polym. Phys. Ed. **20**, 1717 (1982).
[54] R. G. Alamo, L. Mandelkern, G. M. Stack, C. Kröhnke, and G. Wegner, Macromolecules **26**, 2743 (1993).